UDC 551.509.313:551.511.32

A FINITE-DIFFERENCE APPROXIMATION OF THE PRIMITIVE EQUATIONS FOR A HEXAGONAL GRID ON A PLANE

ROBERT SADOURNY and PIERRE MOREL

Laboratoire de Météorologie Dynamique du C.N.R.S., 92–Bellevue–France

ABSTRACT

The hexagonal grid based on a partition of the icosahedron has distinct geometrical qualities for the mapping of a sphere and also presents some indexing difficulties. The applicability of this grid to the primitive equations of fluid dynamics is demonstrated, and a finite-difference approximation of these equations is proposed. The basic variables are the mass fluxes from one hexagonal cell to the next through their common boundary. This scheme conserves the total mass, the total momentum, and the total kinetic energy of the fluid as well as the total squared vorticity of a nondivergent flow. A computational test was performed using a hexagonal grid to describe space periodic waves on a nonrotating plane. The systematic variation of total kinetic and potential energy is less than 10^{-5} after 1,000 time steps.

1. INTRODUCTION

The choice of a particular array of points or grid for representing the flow of a fluid on a sphere is not a simple geometrical problem because a spherical grid should satisfy many conflicting requirements. Basically, the grid should be as uniform as possible and should preserve as well as possible the isotropy of the sphere around any point.

A satisfactory grid can be obtained by mapping the sphere onto a regular icosahedron. The basic grid cell is hexagonal so that *all* grid points are surrounded by six almost equidistant neighbors, *except* for 12 vertices of the icosahedron which have only five neighbors. The resulting hexagonal grid (fig. 1) is remarkably uniform and has no very singular point like the Poles of a Mercator grid. But the hexagonal grid does not allow readily the representation of the flow in terms of zonal and meridional velocity. Indeed, the very concept of zonal or meridional flow is lost here: a "zonal" component of a vector field traced continuously from cell to cell around one vertex is found to turn gradually toward the "meridional" direction (fig. 2). This property is not just a feature of the hexagonal grid but a basic property of any mapping of a curved (spherical) surface onto a plane. To get around this difficulty, we will basically represent the spherical flow by *mass fluxes* between adjacent grid cells. The use of mass fluxes rather than velocity components as the fundamental variables is actually implicit in most space-differencing schemes for numerical integration of the primitive fluid dynamics equations. Bryan (1966) showed under very general geometrical conditions that flux-form difference schemes conserve exactly total momentum and total kinetic energy integrated over the whole sphere, a necessary condition to prevent nonlinear instability of the iteration process (Lilly, 1965). Such conservative schemes are now currently used in numerical weather prediction (Kurihara, 1965; Kurihara and Holloway, 1967).

Furthermore, Arakawa (1966) showed that one particular space-differencing scheme, based on a square grid, conserves total momentum, total kinetic energy, and also the integral of the square of the vorticity for nondivergent flow and thereby does not produce spurious flow of kinetic energy from the cyclone scale toward very long or short wavelengths.

The high degree of isotropy of the hexagonal grid makes the formulation of an energy- and vorticity-conserving scheme simpler, in fact, than for rectangular grids, as shown by Sadourny, Arakawa, and Mintz (1968) for nondivergent barotropic flow.

In the present work, the space-differencing (advection) scheme is first derived in the case of nondivergent flow (section 2); the exact conservation of total momentum kinetic energy and squared vorticity is proved. A consistent definition of the divergence operator is then introduced (section 3), and a complete finite-difference formulation of the primitive dynamic equations is presented for two-

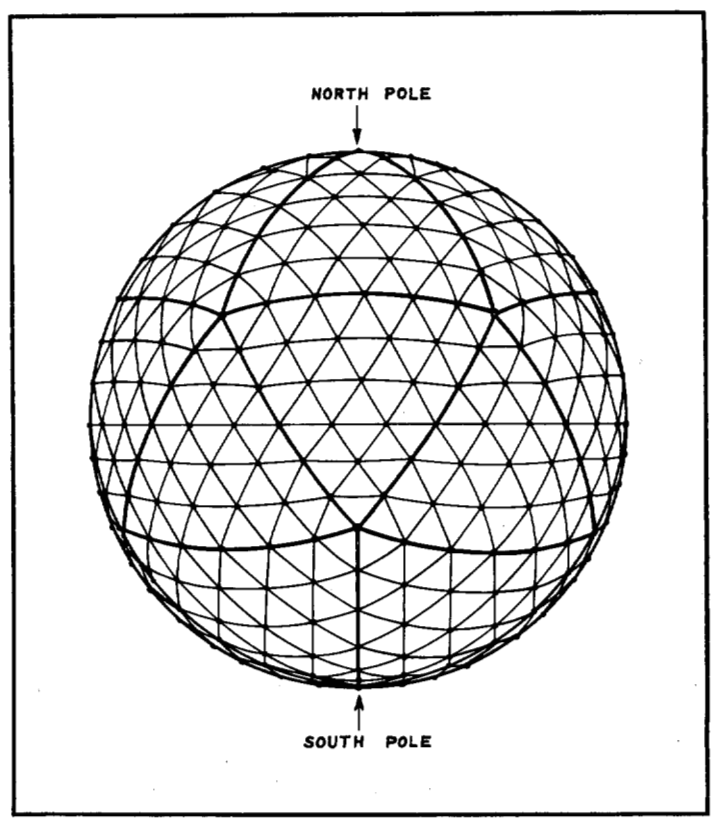

FIGURE 1.—Representation of a 362-point hexagonal grid.

348-966 O—69——4

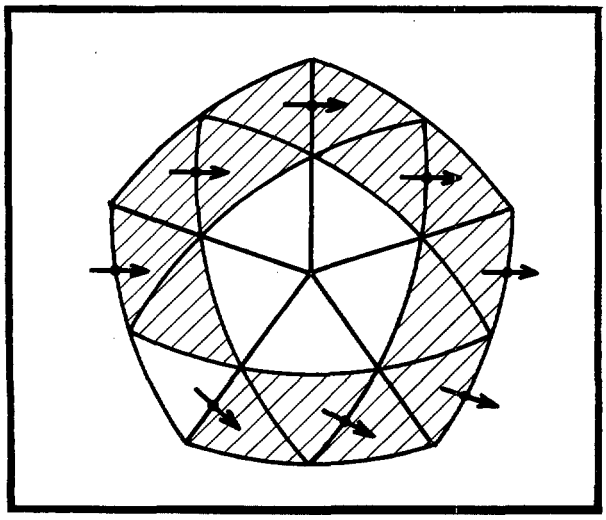

FIGURE 2.—Local orientation of mass fluxes around a pentagon on the spherical grid.

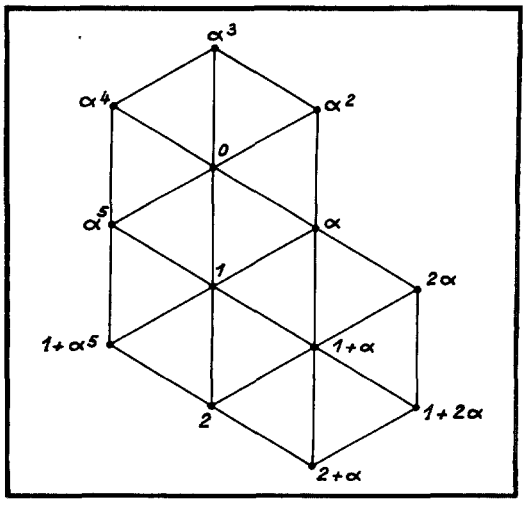

FIGURE 3.—Indexing convention for the hexagonal grid.

dimensional divergent flow on a plane. A simple application to a barotropic flow with a free surface is worked out in section 4, and results of a test computation are discussed.

The modification of the algorithm for pentagonal vertices and, in general, the problem of sphericity corrections in the expression of space derivatives is not discussed here and will be the subject of a later communication.

2. PRIMITIVE DYNAMIC EQUATION FOR NONDIVERGENT FLOW

The geometry of the hexagonal grid on a sphere and the indexing convention used for sample computations have been described by Sadourny, Arakawa, and Mintz (1968). For convenience, we shall now introduce a new indexing convention more suitable for mathematical developments. If the index O is given to one particular grid point chosen as origin, the indices (1), (α), (α^2), . . . , (α^5) designate the six neighbors; α is the complex number $\exp(i\pi/3)$. We shall use the following relations:

$$\begin{aligned}&\alpha^6=\alpha^0=1,\\&\alpha^3=-1,\\&\alpha^i=\alpha^{i+1}+\alpha^{i-1}.\end{aligned}\tag{1}$$

Figure 3 shows how this convention can be applied to any nonsingular sample of the hexagonal grid. It can be readily extended to the surrounding cells in a consistent manner, i.e., the points around grid point (a) are designated by indices ($a+1$), ($a+\alpha$), ($a+\alpha^2$), . . . , ($a+\alpha^5$). Any grid-point index (a) is then a linear combination, with real integer coefficients, of the indices 1, α, . . . , α^5.

The flow velocity is to be defined by mass fluxes between all pairs of neighboring grid points, (a) and ($a+\alpha^i$) for example. The middle of arc (a, $a+\alpha^i$) will be designated by the half-integer index $\left(a+\frac{\alpha^i}{2}\right)$ so that the flux crossing this arc is

$$F(a,\, a+\alpha^i)=dh\left(a+\frac{\alpha^i}{2}\right)u\left(a+\frac{\alpha^i}{2}\right)\tag{2}$$

where h is the density (or the height of the fluid in the case of a divergent barotropic flow) and d is the distance between point (a) and point ($a+\alpha^i$); u is then the component of the flow velocity perpendicular to the arc of great circle (a, $a+\alpha^i$). The velocity field is thus defined on a staggered array by three components u_1, u_2, and u_3 along the axis Ox_1, Ox_2, Ox_3 perpendicular to the sides of the triangular cells (fig. 4).

For simplicity, we discuss in the present article only the case of a regular hexagonal grid made of equal, equilateral triangles. The three axes lie then along the directions O, $2\pi/3$, and $4\pi/3$, and the following identities obtain

$$\begin{aligned}&u_1(a)+u_2(a)+u_3(a)=0\\\text{and}\qquad&\\&\tfrac{1}{3}\{u_1^2(a)+u_1^2(a)+u_3^2(a)\}=\tfrac{1}{2}|\mathbf{V}(a)|^2.\end{aligned}\tag{3}$$

This leads to a reasonable definition for the *kinetic energy* K:

$$K=\frac{s}{9}\sum_a\sum_{i=1}^{3}hu^2\left(a+\frac{\alpha^i}{2}\right)\tag{4}$$

where s is the area of the hexagonal cell. Note that the sum of all overlapping hexagons is 3 times the area covered by the grid (hence the factor $\frac{1}{9}$). Similarly, the *momentum* in the direction Ox_i perpendicular to the grid side (a, $a+\alpha^i$) is then

$$P_i=\frac{s}{3}\sum_a hu\left(a+\frac{\alpha^i}{2}\right).\tag{5}$$

The mean value of the flow vorticity ζ in a cell can be expressed by the circulation of the flow velocity around it divided by the cell area. For consistency, we choose here a smaller hexagonal cell depicted in figure 5, and the following finite-difference approximation obtains

$$\zeta(a)=\frac{d\sqrt{3}}{s}\sum_{i=1}^{6}u\left(a+\frac{\alpha^i}{2}\right).\tag{6}$$

Consider now the fundamental equation of fluid dynamics or more precisely the contribution of horizontal advection to the Eulerian time derivative:

$$\frac{\partial(hu)}{\partial t}+\nabla\cdot(hu\,\mathbf{V})=0\tag{7}$$

where u is the velocity component along a given direction,

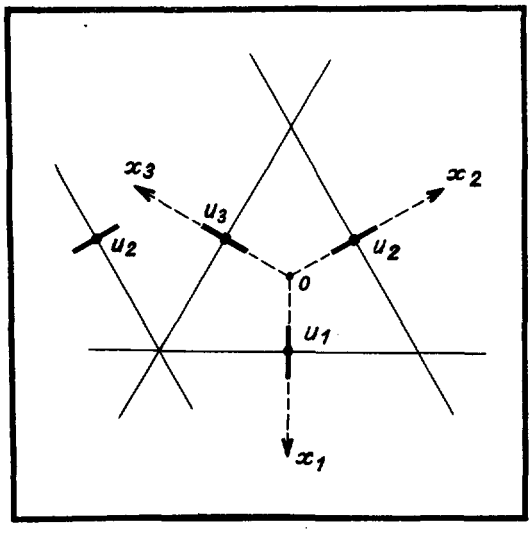

FIGURE 4.—Locations for wind components.

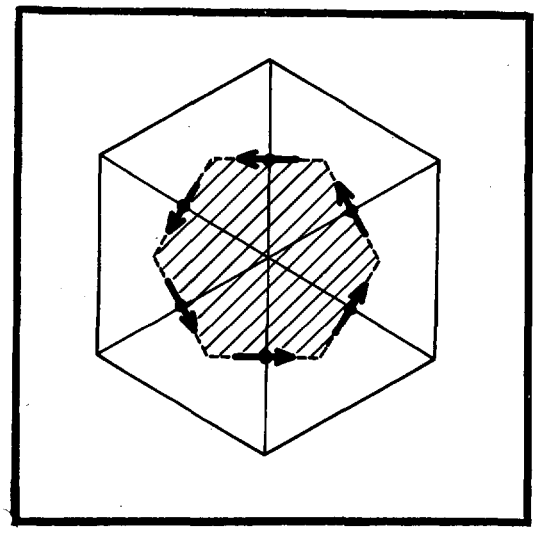

FIGURE 5.—Representation of vorticity at a grid point.

and the vertical advection, Coriolis acceleration, and source terms are neglected for the time being. For *non-divergent flow*, h is constant and one may introduce a stream function ψ such that

$$\mathbf{k}\times h\,\mathbf{V}=\nabla\psi$$

and

$$F(a,a+\alpha^i)=\psi(a+\alpha^i)-\psi(a). \tag{8}$$

Expressing (7) in terms of the stream function, ψ, it follows that

$$\partial(hu)/\partial t=J(u,\psi). \tag{9}$$

$J(u,\psi)$ is the Jacobian operator applied to the scalar fields u and ψ. This last relation is formally identical to the barotropic vorticity equation treated by Sadourny, Arakawa, and Mintz (1968). We shall, therefore, use the same finite-difference approximation J_* for the Jacobian operator, i.e.,

$$\partial(hu)/\partial t=J_*(u,\psi) \tag{10}$$

and

$$J_*(u,\psi)=\frac{1}{2s}\sum_j[u(b)+u(b+\alpha^j)][\psi(b+\alpha^{j+1})-\psi(b+\alpha^{j-1})], \tag{11a}$$

or the equivalent form

$$J_*(u,\psi)=\frac{1}{2s}\sum_j u(b+\alpha^j)[\psi b+\alpha^{j+1})-\psi(b+\alpha^{j-1})]. \tag{11b}$$

Note that the field u is defined at half-integer points $b=a+\frac{\alpha^i}{2}$ (see fig. 6), whereas the stream function is defined at normal grid points $(a+\alpha^i)$. We shall come back to this difficulty later. This finite-difference advection operator conserves exactly the total momentum (5), as can be seen with the help of equations (10) and (11a):

$$\frac{\partial P}{\partial t}=\frac{s}{3}\sum_b\frac{\partial}{\partial t}hu(b)$$

$$=\frac{s}{3}\sum_b\sum_j[u(b)+u(b+\alpha^j)][\psi(b+\alpha^{j+1})-\psi(b+\alpha^{j-1})]. \tag{12}$$

The first bracket is symmetrical with respect to the interchange of indices (b) and $(b+\alpha^j)$. The second bracket is antisymmetrical since the same flux across arc $(b+\alpha^{j-1}, b+\alpha^{j+1})$ appears in the expression of $J_*(b+\alpha^j)$ but in the reverse direction (fig. 7). Thus, the sum on the right-hand side of equation (12) cancels exactly with periodic boundary conditions or on a closed surface:

$$\partial P/\partial t=0.$$

A similar argument shows for each of the three directions Ox_i that the contribution of u_i components to the total kinetic energy is also conserved exactly. We get from equations (4), (10), and (11b):

$$\frac{\partial}{\partial t}\left[\frac{s}{9}\sum_b hu^2(b)\right]=\frac{2s}{9}\sum_b u(b)J_*(u,\psi)$$

$$=\frac{2s}{9}\sum_b\sum_j[u(b)\cdot u(b+\alpha^j)][\psi(b+\alpha^{j+1})-\psi(b+\alpha^{j-1})]. \tag{13}$$

Again, the first bracket is symmetrical with respect to (b) and $(b+\alpha^j)$, and the sum on the right-hand side cancels exactly in a closed domain. The total kinetic energy is thus exactly conserved by the advection scheme (11):

$$\partial K/\partial t=0.$$

These properties are common to all space-differencing schemes expressed in momentum flux divergence form (Bryan, 1966). We shall show that the total squared vorticity of the flow is also conserved in the case of nondivergent barotropic flow. In fact it is sufficient to show that in that case equation (10) is equivalent to the finite-difference vorticity equation

$$\partial\zeta(a)/\partial t=J_*(\zeta,\psi). \tag{14}$$

Indeed, using expression (6) of the vorticity together with equation (10), we get

$$\frac{\partial\zeta}{\partial t}(a)=\frac{d\sqrt{3}}{s}\sum_{i=1}^{6}\frac{\partial}{\partial t}u\left(a+\frac{\alpha^i}{2}\right)$$

$$=\frac{d\sqrt{3}}{2hs^2}\sum_{i=1}^{6}\sum_{j=1}^{6}u\left(a+\frac{\alpha^i}{2}+\alpha^j\right)\left[\psi\left(a+\frac{\alpha^i}{2}+\alpha^{j+1}\right)-\psi\left(a+\frac{\alpha^i}{2}+\alpha^{j-1}\right)\right]. \tag{15}$$

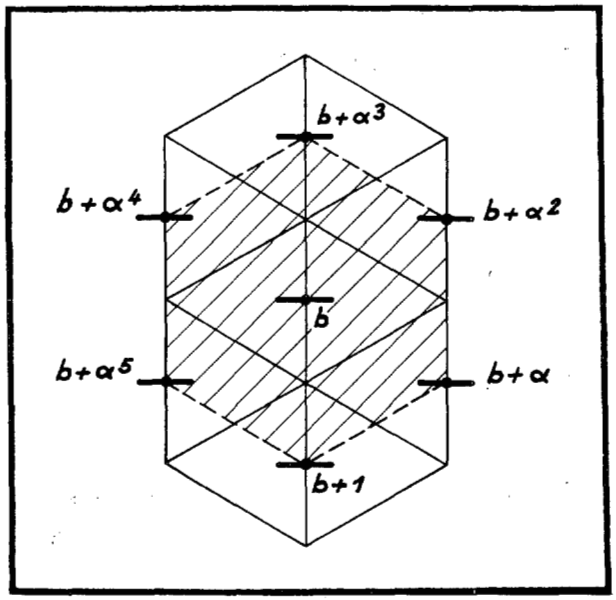

FIGURE 6.—Wind components used in the momentum advection scheme.

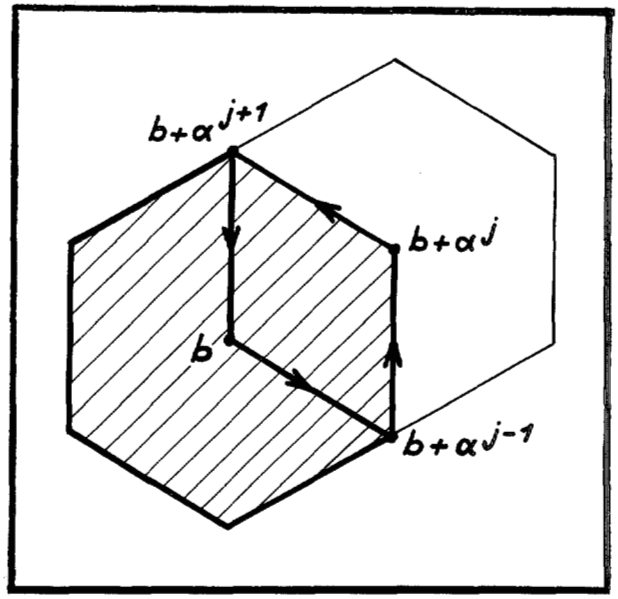

FIGURE 7.—Antisymmetry of the flux between (b) and $(b+\alpha^i)$.

In this equation, the values of the stream function at half-integer points must be interpolated from the neighboring grid points, viz:

$$\psi\left(a+\frac{\alpha^i}{2}\right)=\frac{1}{2}[\psi(a)+\psi(a+\alpha^i)]=\psi(a)+\frac{1}{2}\times[\psi(a+\alpha^i)-\psi(a)]=\psi(a)+\frac{d}{2}u\left(a+\frac{\alpha^i}{2}\right) \quad (16)$$

where the definitions (2) and (8) have been used. Thus,

$$\frac{\partial\zeta}{\partial t}(a)=\frac{d\sqrt{3}}{2hs^2}\sum_{i=1}^{6}\sum_{j=1}^{6}u\left(a+\frac{\alpha^i}{2}+\alpha^j\right)[\psi(a+\alpha^{j+1})-\psi(a+\alpha^{j-1})]+\frac{d^2\sqrt{3}}{4hs^2}\sum_{i=1}^{6}\sum_{j=1}^{6}u\left(a+\frac{\alpha^i}{2}+\alpha^j\right)\left[u\left(a+\frac{\alpha^i}{2}+\alpha^{j+1}\right)-u\left(a+\frac{\alpha^i}{2}+\alpha^{j-1}\right)\right].$$

Note that the second term on the right-hand side is exactly

$$\frac{d^2\sqrt{3}}{2hs}\sum_{i=1}^{6}[J_*(u,u)]_{a+\frac{\alpha^i}{2}}.$$

Each term $J_*(u,u)$ cancels exactly; hence, equation (15) reduces to

$$\frac{\partial\zeta}{\partial t}(a)=\frac{1}{2s}\sum_{j=1}^{6}[\psi(a+\alpha^{j+1})-\psi(a+\alpha^{j-1})]\frac{d\sqrt{3}}{s}\sum_{i=1}^{6}u\left(a+\frac{\alpha^i}{2}+\alpha^j\right)$$

$$=\frac{1}{2s}\sum_{j=1}^{6}\zeta(a+\alpha^j)[\psi(a+\alpha^{j+1})-\psi(a+\alpha^{j-1})]$$

or

$$\partial\zeta(a)/\partial t=J_*(\zeta,\psi). \quad (17)$$

We have introduced a finite-difference approximation of the momentum flux divergence term $\nabla\cdot(hu\mathbf{V})$ of the primitive dynamic equation. The flux form insures the conservation of the total momentum and kinetic energy. This differencing scheme involves equally the six nearest points where the same components of the velocity are defined. By summing the six u-components $u\left(a+\frac{a^i}{2}\right)$ around grid point (a), we find that the same advection scheme also applies to the circulation around grid points (vorticity). This scheme is, therefore, consistent with the particular form of the barotropic vorticity equation studied by Sadourny, Arakawa, and Mintz (1968); this form conserves exactly the total vorticity and squared vorticity of a nondivergent flow.

3. DIVERGENT FLOW

Let us consider now a simple barotropic flow with a free surface, and let h be the variable depth of the (incompressible) fluid. The continuity equation and the equation of motion along a given direction are

$$\frac{\partial h}{\partial t}+\nabla\cdot(h\mathbf{V})=0 \quad (18)$$

and

$$\frac{\partial(hu)}{\partial t}+\nabla\cdot(hu\mathbf{V})+\frac{\partial}{\partial x}\left(\frac{1}{2}gh^2\right)=0. \quad (19)$$

The momentum advection algorithm developed in the previous section is not yet in a generally usable form since the stream function still appears in equations (10) and (11). For a more general flow, we shall introduce instead the corresponding mass flux (dashed segment in fig. 8). Thus,

$$\frac{\partial}{\partial t}(hu)\left(a+\frac{\alpha^i}{2}\right)=\frac{1}{2s}\sum_{j=1}^{6}\left[u\left(a+\frac{\alpha^i}{2}\right)+u\left(a+\frac{\alpha^i}{2}+\alpha^j\right)\right]F\left(a+\frac{\alpha^i}{2}+\alpha^{j-1},\ a+\frac{\alpha^i}{2}+\alpha^{j+1}\right). \quad (20)$$

The mass fluxes are only defined normally across triangle sides. The interpolation formula to give mass flux along

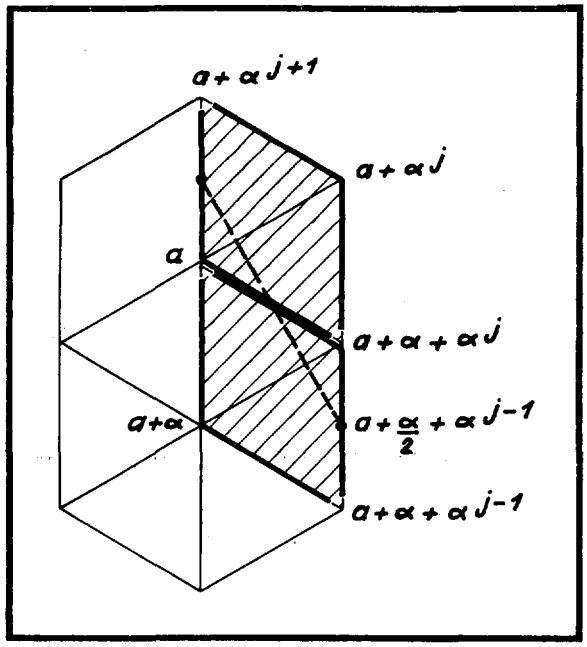

FIGURE 8.—Representation of a mass flux used in momentum advection scheme.

the dashed line in figure 8 is found to be the mean value of the four fluxes across the heavy lines of figure 8, viz:

$$F\left(a+\frac{\alpha^i}{2}+\alpha^{j-1},\ a+\frac{\alpha^i}{2}+\alpha^{j+1}\right)$$
$$=\tfrac{1}{4}[F(a+\alpha^{j-1},\ a)+F(a,a+\alpha^{j+1})$$
$$+F(a+\alpha^{j-1},\ a+\alpha^j)+F(a+\alpha^j,\ a+\alpha^{j+1})$$
$$+F(a+\alpha^i+\alpha^{j-1},\ a+\alpha^i)+F(a+\alpha^i,\ a+\alpha^i+\alpha^{j+1})$$
$$+F(a+\alpha^i+\alpha^{j-1},\ a+\alpha^i+\alpha^j)$$
$$+F(a+\alpha^i+\alpha^j,\ a+\alpha^i+\alpha^{j+1})]. \quad (21)$$

In this form, the advection term is still defined as the divergence of a *mass flux*, and the conservation of total momentum obtains even when the depth h is variable. Concerning the conservation of kinetic energy, we derive from equations (4), (10), and (20) the relation

$$\frac{\partial K}{\partial t}=\frac{s}{9}\sum_a\sum_{i=1}^{3}\left[2u\left(a+\frac{\alpha^i}{2}\right)\frac{\partial}{\partial t}(hu)-u^2\left(a+\frac{\alpha^i}{2}\right)\frac{\partial h}{\partial t}\right]$$
$$=\frac{s}{9}\sum_a\sum_{i=1}^{3}\left[\frac{1}{s}\sum_{j=1}^{6}u^2\left(a+\frac{\alpha^i}{2}\right)F\left(a+\frac{\alpha^i}{2}+\alpha^{j-1},a+\frac{\alpha^i}{2}+\alpha^{j+1}\right)\right.$$
$$+\frac{1}{s}\sum_{j=1}^{6}u\left(a+\frac{\alpha^i}{2}\right)u\left(a+\frac{\alpha^i}{2}+\alpha^j\right)F\left(a+\frac{\alpha^i}{2}+\alpha^{j-1},a+\frac{\alpha^i}{2}\right.$$
$$\left.\left.+\alpha^{j+1}\right)-u^2\left(a+\frac{\alpha^i}{2}\right)\frac{\partial h}{\partial t}\left(a+\frac{\alpha^i}{2}\right)\right]. \quad (22)$$

We have seen in section 2 that the second sum on the right-hand side of equation (22) cancels exactly. Consequently, the total kinetic energy will be conserved if and only if we use the following finite-difference approximation of the continuity equation:

$$\frac{\partial}{\partial t}h\left(a+\frac{\alpha^i}{2}\right)=\frac{1}{s}\sum_{j=1}^{6}F\left(a+\frac{\alpha^i}{2}+\alpha^{j-1},a+\frac{\alpha^i}{2}+\alpha^{j+1}\right).$$

In fact, the height h is normally defined at integer grid points only. Using linear interpolation to define its value at half-integer points $\left(a+\frac{\alpha^i}{2}\right)$ we get

$$\frac{\partial h}{\partial t}(a)=\frac{1}{s}\sum_{j=1}^{6}F(a+\alpha^{j-1},\ a+\alpha^{j+1}). \quad (23)$$

To be consistent with equation (21), we shall replace the fluxes on the right-hand side of (23) by linear combinations,

$$F(a+\alpha^{j-1},\ a+\alpha^{j+1})=\tfrac{1}{2}[F(a+\alpha^{j-1},\ a)+F(a,\ a+\alpha^{j+1})$$
$$+F(a+\alpha^{j-1},\ a+\alpha^j)+F(a+\alpha^j,\ a+\alpha^{j+1})]. \quad (24)$$

We note, however, that the fluxes through the radial segments ($F(a,a+\alpha^j)$ cancel; the sum on the right-hand side of equation (23) reduces finally to

$$\frac{\partial h(a)}{\partial t}=\frac{1}{s}\sum_{j=1}^{6}F(a+\alpha^j,\ a+\alpha^{j+1}). \quad (25)$$

The consistent finite-difference approximation of the divergence of the flow is, therefore, the total mass flux through the sides of the hexagonal side (fig. 9) divided by the surface of the cell.

Next we have to consider the exchange between kinetic and potential energy, and specify the finite-difference approximation of the pressure gradient so that total energy will be conserved. From equation (25), the elementary flux $F(a+\alpha^j,\ a+\alpha^{j+1})$ acts upon two height tendencies in the following manner: $F(a+\alpha^j,\ a+\alpha^{j+1})$ is added to $s\frac{\partial h(a)}{\partial t}$ and subtracted from $s\frac{\partial h(a+\alpha^j+\alpha^{j+1})}{\partial t}$. Its contribution to the total potential energy tendency is thus:

$$gF(a+\alpha^j,\ a+\alpha^{j+1})[h(a)-h(a+\alpha^j+\alpha^{j+1})]$$
$$=gdh\left(a+\frac{\alpha^j+\alpha^{j+1}}{2}\right)u\left(a+\frac{\alpha^j+\alpha^{j+1}}{2}\right)[h(a)$$
$$-h(a+\alpha^j+\alpha^{j+1})].$$

This term can also be understood as the contribution of the pressure gradient at point $\left(a+\frac{\alpha^j+\alpha^{j+1}}{2}\right)$ to the kinetic energy tendency at the same point, if the gradient term in equation (19) is written at point $\left(a+\frac{\alpha^j+\alpha^{j+1}}{2}\right)$ in the following manner:

$$\frac{3d}{2s}gh\left(a+\frac{\alpha^j+\alpha^{j+1}}{2}\right)[h(a+\alpha^j+\alpha^{j+1})-h(a)].$$

With this definition, the scheme enforces the exchange between potential and kinetic energy without loss.

4. COMPUTATIONAL TEST

As a test case, we have chosen to integrate equations (18) and (19) for divergent barotropic flow to simulate the propagation and multiple reflexions of periodic gravity waves in a channel. The channel can be pictured as an equatorial belt around a nonrotating planet (the Coriolis

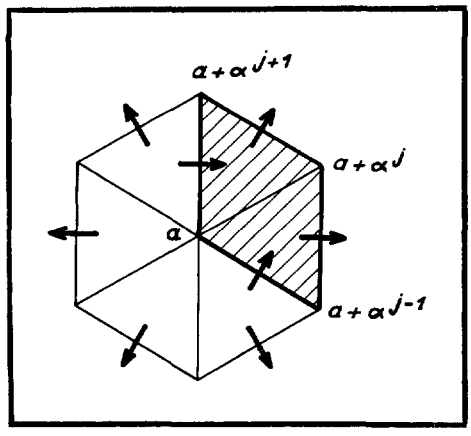

FIGURE 9.—Representation of divergence at a grid point.

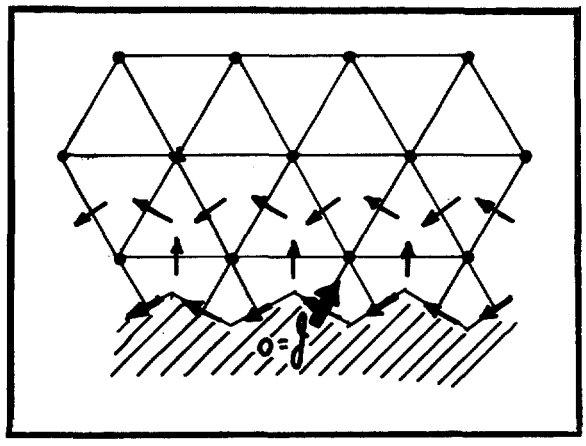

FIGURE 10.—Boundary of the grid in the channel case.

acceleration is omitted for the time being). The north and south boundaries are perfect walls without friction (free slip boundary). The waves propagate in the east-west direction. The computational test was carried out in one section of the channel only, and periodic boundary conditions on the east and west boundaries were assumed, thereby enforcing an exact space periodicity.

The application of the differencing scheme is straightforward where the free-slip boundary condition is introduced properly, i.e., in a way consistent with the conservation of all integral constraints. In view of the geometry of the grid and the definition of the basic F fluxes, the boundary must be taken on a polygonal line as shown in figure 10. If so, two different classes of boundary fluxes appear in the computation:

1) Flux parallel to the boundary defined at a point $\left(a+\frac{\alpha^j}{2}\right)$ of the boundary. All such fluxes are included as dependent variable and actually computed on each time step according to the general scheme (21).

2) Flux perpendicular to the boundary defined at a point $\left(a+\frac{\alpha^j}{2}\right)$ of the boundary. All such fluxes are set equal to zero.

Needless to say, all fluxes defined on the other side of the boundary are also set equal to zero. These specifications, therefore, add up to the elimination of any inflow or outflow of mass, momentum, and kinetic energy across the boundary.

EXPERIMENT A

This test was carried out on a square domain including 10 by 10 hexagonal cells and the same number of grid points. The grid size d was chosen equal to 100 km. The fluid was assumed to be initially at rest (V=0) with a wavy surface defined by the field (unit: meter),

$$h(x,y)=10^4+10^3\times\sin\frac{\pi y}{L}+300\times\sin\frac{2\pi x}{L}.$$

The initial energy of the system is thus purely potential energy. The subsequent integration of the equations of motions will show a quasi-periodic interchange between potential and kinetic energy corresponding to the propagation and reflexion of these waves.

Because the test is intended to verify the conservation of energy, the use of a nonamplifying time-differencing scheme is mandatory. Time integration was, therefore, carried out with the centered or "leapfrog" scheme:

$$q(t+1)=q(t-1)+2\Delta t\frac{\partial q}{\partial t}(t)$$

except, of course, for the first time step for which the Euler-backward or Matsuno scheme was used:

$$q^*(1)=q(0)+\Delta t\frac{\partial q}{\partial t}(0)$$

and

$$q(1)=q^*(1)+\Delta t\left[\frac{\partial q^*}{\partial t}(1)-\frac{\partial q}{\partial t}(0)\right].$$

The problem of the one-dimensional free surface flow corresponding to this situation is solved by introducing characteristic lines with slopes

$$dx/dt=u\pm\sqrt{gh}.$$

The stability criterium for time integration is thus:

$$\Delta t<\frac{\Delta x}{|u\pm\sqrt{gh}|}.$$

Here Δx is 10^5 m, $\sqrt{gh}$ is about 300 m sec^{-1}, and the mean flow velocity can be neglected. The stability criterium is then

$$\Delta t<300 \text{ sec}.$$

Time steps of 240 sec were actually used.

EXPERIMENT B

Experiment B differs from experiment A by the size of the domain, the initial state, and a more refined starting procedure. The domain considered here includes 20 by 20 grid points with the same grid size d: 100 km. The initial state is defined by the field values

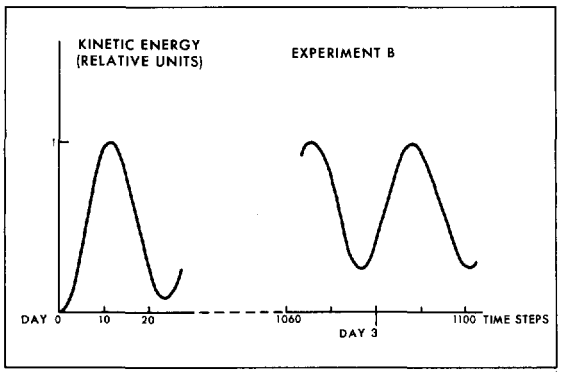

FIGURE 11.—Behavior of total kinetic energy with time.

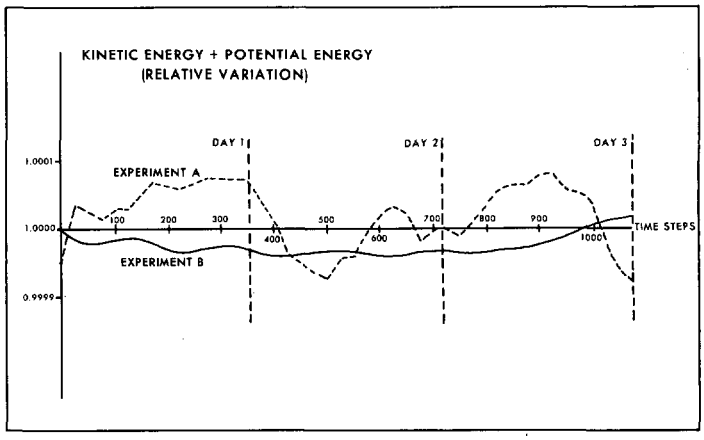

FIGURE 12.—Variation of total energy.

$$h(x,y)=10^4+10^3\times\sin\frac{\pi y}{L}\times\sin\frac{2\pi x}{L}+300\times\sin\frac{2\pi y}{L}\times\sin\frac{4\pi x}{L}$$

and

$$V(x,y)=0.$$

The first time-integration step was performed according to a more accurate, second-order approximation consisting in:

a forward integration from $t=0$ to $t=\frac{1}{2}$

and

a Euler-backward step from $t=\frac{1}{2}$ to $t=1$

when applied to sinusoidal solutions of equation $dx/dt=i\omega x$. This second-order scheme has an amplification coefficient which is very close to 1,

$$A=\left[1+\left(\frac{\omega\Delta t}{2}\right)^6\right]^{1/2}.$$

RESULT

In both cases, the integration of the equations of motion indicates a quasi-periodic exchange between kinetic and potential energy corresponding to the propagation and reflection of the large-scale (order L) waves. The model does not include any dissipation process and, consequently, nonlinear interaction between the spectral components represented by the grid produces a steadily growing high-frequency spectrum. Although the total kinetic energy peaks are remarkably constant after several days, the large-scale oscillation amplitude decreases significantly; whereas, the high-frequency kinetic energy (appearing as a practically constant "noise") increases by a corresponding amount (fig. 11).

The total mass is exactly conserved except for systematic truncation errors due to the computer system; the truncation errors produce a slight linear mass loss which amounts to 10^{-4} after 1,000 time steps.

The variation of total (kinetic+potential) energy is shown in figure 12. Curve A is drawn using values computed every 25 time steps without smoothing to remove the high-frequency oscillation characteristic of the centered time-differencing scheme. This smoothing was done for curve B. The systematic variation of total energy appears to be somewhat less than 10^{-5} in 1,000 time steps.

ACKNOWLEDGMENTS

The basic formulation used here is inspired by the work of A. Arakawa. We want to express our gratitude for his very helpful comments and suggestions. We are also much indebted to the Centre National d'Etudes Spatiales of France for computing facilities. We acknowledge here the good will of the C.N.E.S. computing center personnel.

REFERENCES

Arakawa, A., "Computational Design for Long-Term Numerical Integration of the Equations of Fluid Motion: Two Dimensional Incompressible Flow Part I.," *Journal of Computational Physics*, Vol. 1, No. 1, Academic Press, New York, Aug. **1966**, pp. 119–143.

Bryan, K., "A Scheme for Numerical Integration of the Equations of Motion on an Irregular Grid Free of Nonlinear Instability," *Monthly Weather Review*, Vol. 94, No. 1, Jan. **1966**, pp. 39–40.

Kurihara, Y., "Numerical Integration of the Primitive Equations on a Spherical Grid," *Monthly Weather Review*, Vol. 93, No. 7, July **1965**, pp. 399–415.

Kurihara, Y., and Holloway, J. L., Jr., "Numerical Integration of a Nine-Level Global Primitive Equations Model Formulated by the Box Method," *Monthly Weather Review*, Vol. 95, No. 8, Aug. **1967**, pp. 509–530.

Lilly, D. K., "On the Computational Stability of Numerical Solutions of Time-Dependent Non-Linear Geophysical Fluid Dynamics Problems," *Monthly Weather Review*, Vol. 93, No. 1, Jan. **1965**, pp. 11–26.

Sadourny, R., Arakawa, A., and Mintz, Y., "Integration of the Nondivergent Barotropic Vorticity Equation With an Icosahedral-Hexagonal Grid for the Sphere," *Monthly Weather Review*, Vol. 96, No. 6, June **1968**, pp. 351–356.

[*Received September 9, 1968; revised October 28, 1968*]